Research Article

Maha Abdallah Alnuwaiser, Mohamed Rabia*

# Hollow mushroom nanomaterials for potentiometric sensing of $Pb^{2+}$ ions in water via the intercalation of iodide ions into the polypyrrole matrix

https://doi.org/10.1515/chem-2024-0217
received November 8, 2023; accepted February 23, 2024

**Abstract:** Herein, the synthesis of a sensor for the determination of lead ($Pb^{2+}$) ions via the intercalation of iodide ions into the polypyrrole matrix is performed. It demonstrated a Nernstian slope of 31.7 mV/decade, indicating a linear response within the concentration range of $10^{-5}$–$10^{-1}$ M. The detection limit achieved is $9.10^{-6}$ M, indicating the sensor's sensitivity to low concentrations of $Pb^{2+}$. The effectiveness of the Ppy/$I^-$ sensor in $Pb^{2+}$ sensing is confirmed through cyclic voltammetry, where a peak potential of −0.2 V is observed. The sensitivity of the sensor for $Pb^{2+}$ detection is measured to be 2 μA/M. Moreover, the Ppy/$I^-$ sensor exhibits a negative response to interfering ions, which enhances its selectivity for $Pb^{2+}$ detection. Furthermore, when tested with natural water samples such as tap or underground water, which are typically free of lead ions, the sensor demonstrates a negative response to normal interfering ions commonly found in such samples. The Ppy/$I^-$ sensor offers several advantages, including the ability to detect $Pb^{2+}$ ions at very low concentrations, a flexible and adaptable design, and a cost-effective preparation technique. These features make it a promising tool for accurate and efficient detection of $Pb^{2+}$ ions.

**Keywords:** hollow mushroom nanomaterials, polypyrrole, potentiometric, $Pb^{2+}$ ions, sensor

*** Corresponding author: Mohamed Rabia,** Nanomaterials Science Research Laboratory, Chemistry Department, Faculty of Science, Beni-Suef University, Beni-Suef, 62514, Egypt,
e-mail: mohamedchem@science.bsu.edu.eg
**Maha Abdallah Alnuwaiser:** Department of Chemistry, College of Science, Princess Nourah Bint Abdulrahman University, P.O. Box 84428, Riyadh, 11671, Saudi Arabia, e-mail: maalnoussier@pnu.edu.sa

## 1 Introduction

Lead is a soft, heavy metal that is very toxic and dangerous to human life in all environments. It affects children greatly because they are more sensitive and susceptible to it, and it causes poisoning that leads to damage to the internal organs and causes growth retardation and behavioral problems [1]. Several strategies have been devised for the detection of lead in various samples. However, it is worth noting that many of these methods and techniques are associated with significant financial costs and require intricate and costly equipment for operation and maintenance. Additionally, some of these techniques may also result in sample consumption [2–4]. Potential sensors constitute one of the most important and least expensive classes of chemical sensors today. The application of measuring voltage sensors, which range between degrees in relation to the size of the concentration, is an important advantage in this analytical technique, in addition to its simplicity for the wall of the voltage sensors in solution. The electrodes composed of these membranes are called ion-selective electrodes. These selective electrical systems increasingly use ionic species and nanomaterials [5,6]. These systems are classified into two types according to their structural form: symmetric and non-symmetric.

The use of polymers in detecting heavy metals holds great promise due to the strong coordination bonds formed between the electronegative atoms in the polymer and the positive charge of metal ions [7]. Certain categories of polymers, such as aniline and its derivatives, pyrrole, or thiophene derivatives, exhibit desirable characteristics such as cost-effectiveness, good mechanical properties, and semiconductivity. These polymer categories have demonstrated their applicability in various commercial and industrial applications.

To further amplify the benefits of using polymer materials for the detection of heavy metals, there are two

strategies that can be employed. First, one can pursue the synthesis of polymers with specific morphological characteristics, such as porous structures, rods, or fibers. This approach holds the potential to substantially elevate their performance [12,13]. The rationale behind this lies in the fact that tailored morphologies offer advantages like an expanded surface area, which in turn facilitates more effective interactions with heavy metal ions.

The second avenue involves the incorporation of additional substances into the polymer materials, a process known as doping. This deliberate introduction of dopants or additives can yield significant enhancements in the electrical and mechanical properties of the polymers. As a result, the overall performance of these polymers in heavy metal detection applications can be greatly improved.

Polypyrrole (Ppy) polymer exhibits remarkable morphological and semiconductor properties, making it highly effective for a wide range of applications [8]. The Ppy materials demonstrate an intriguing strain behavior that can be integrated into polyurethane nanocomposites. This unique strain behavior provides an avenue to enhance the mechanical properties of different materials, with the observed strain reaching as high as 10% [9]. Also, a composite consisting of Ppy, polycaprolactone, and β-cyclodextrin, characterized by its fibrous morphological properties, is employed for the electrochemical detection of dinotefuran. This sensor achieves an impressive detection limit of 0.05 μM [10]. Furthermore, Ppy finds an electrochemical application as a sensor for detecting SARS-CoV-2-S. In this particular study, PPy is deposited onto a Pt–metal substrate to enable this sensing approach [11]. Also, the oxidation of pyrrole is carried out using ferric chloride ($FeCl_3$), resulting in the formation of a porous composite known as polypyrrole–iron composite (Ppy–Fe). This composite is utilized as a sensor for detecting ammonia ($NH_3$) gas [12].

Several prior research studies have explored the detection of heavy metals using various techniques and sensor systems. Here is a summary of some of these notable studies:

Triviño et al. [13] conducted research on potentiometric sensors with the aim of enhancing their properties for heavy metal detection. The study likely involved improvements in sensor sensitivity, selectivity, and response time, which are crucial factors in effective detection methods. In another study, researchers investigated the use of a hanging mercury electrode and a glassy carbon electrode modified with Nafion–mercury (Hg) for the detection of $Pb^{2+}$ and cadmium ($Cd^{2+}$) ions. Their approach was based on adsorption voltammetry, and quercetin-5′-sulfonic acid was likely used as a reagent to facilitate the detection process. This method may have provided insights into the electrochemical behavior of these heavy metal ions [13]. Ghaedi et al. [14] developed an ion-selective electrode specifically designed for the detection of $Pb^{2+}$ ions. This electrode was based on a chemical compound named 1-((3-((2-hydroxynaphthalen-1-yl)methyleneamino)-2,2-dimethylpropylimino)methyl)naphthalen-2-ol. The research likely focused on optimizing the electrode's variables to achieve maximum sensitivity and accuracy. The electrode's performance was assessed over a range of pH values, and the study reported a response slope of 25.79 mV/decade within the pH range of 5.0–7.2.

Ikena et al. [15] explored the fabrication of new thin-film polymeric materials for the detection of $Pb^{2+}$ and $Cd^{2+}$ ions. This research aimed to develop innovative sensor materials that could offer improved sensitivity and selectivity for these heavy metal ions. The reported response slopes of 23.9 mV/decade for $Pb^{2+}$ and 25.5 mV/decade for $Cd^{2+}$ ions suggest that these sensors exhibited promising detection capabilities for a relatively wide concentration range of these heavy metals [16,17].

In this study, an efficient Ppy/$I^-$ sensor is developed using a cost-effective method that involves oxidizing pyrrole with iodine as the oxidant. The exceptional sensing capability of this sensor for $Pb^{2+}$ ions can be attributed to either the unique morphology resembling hollow mushrooms or the strong interaction between the nanomaterials and $Pb^{2+}$ ions.

The sensitivity of the Ppy/$I^-$ sensor towards $Pb^{2+}$ ions is demonstrated through two techniques: simple and cyclic voltammetry techniques. Both methods complement each other and provide consistent results. The sensor exhibits a significant Nernstian slope, indicating a linear response over a concentration range of $10^{-5}$–$10^{-1}$ M. Additionally, using cyclic voltammetry, the sensor displays excellent sensitivity within a concentration range of $10^{-4}$–$10^{-1}$ M.

Importantly, the Ppy/$I^-$ sensor shows no interference or interaction with other ions present in lead-free natural samples like tap or underground water. This highlights the sensor's selectivity for $Pb^{2+}$ ions and its ability to distinguish them from other elements commonly found in environmental samples.

Therefore, the prepared Ppy/$I^-$ sensor offers an efficient and cost-effective solution for detecting $Pb^{2+}$ ions. Its unique morphology or strong interaction with $Pb^{2+}$ ions, along with the corroborating results from simple and cyclic voltammetry, demonstrates its reliable performance. Additionally, the sensor exhibits high selectivity toward $Pb^{2+}$ ions, making it suitable for the accurate detection of $Pb^{2+}$ in various environmental samples, including lead-free water sources.

# 2 Materials and methods

## 2.1 Materials

Iodine, sodium hydroxide (NaOH, 99.9%), and acetic acid ($CH_3COOH$, 99.8%) were procured from Pio Chem Company, Egypt. $Pb(NO_3)_2$ (99.9%) was sourced from El-Naser Chemical Company, Egypt. Pyrrole was obtained from Sigma Aldrich, Japan. Additionally, hydrochloric acid (HCl, 36%) was purchased from Merck, Germany.

## 2.2 Ppy/$I^-$ nanocomposite thin film sensor preparation

The synthesis of polypyrrole (Ppy) involves the formation of pyrrole radicals through an oxidation reaction using potassium persulfate ($K_2S_2O_8$) as the oxidant [18]. Initially, pyrrole is dissolved in a 0.5 M HCl acidic solution under stirring. The addition of the $K_2S_2O_8$ oxidant directly to the solution results in the formation of Ppy nanoparticles. As pyrrole radicals are generated, they subsequently undergo mutual attack to facilitate the creation of Ppy. The outcome is the precipitation of a green substance, denoted as Ppy, which is further subjected to thorough washing and subsequent warm drying.

For the preparation of the PPy/$I^-$ nanocomposite thin film sensor based on the glass substrate, pyrrole is oxidized using iodine as the oxidant. In this case, 0.06 M pyrrole is dissolved in a 1 M acetic acid solution. The oxidation process leads to the intercalation of iodide ions between the Ppy chains, forming the PPy/$I^-$ nanocomposite, which is utilized for sensing applications after additional treatments, including washing and drying at 60°C.

## 2.3 Potentiometric sensing

The Ppy/$I^-$ nanocomposite thin film sensor demonstrates the potential for detecting $Pb^{2+}$ ions. The intercalation of iodide ions within the Ppy chains facilitates additional ion interactions with the sensor in solution. Detection is carried out using a simple potentiometric method, employing a two-electrode cell with the PPy/$I^-$ nanocomposite thin film as the sensing electrode. Cyclic voltammetry, utilizing a three-electrode cell, is utilized to detect $Pb^{2+}$ ions by analyzing the resulting cyclic voltammetry curves, where the peak height corresponds to the $Pb^{2+}$ ion concentration. Both these methods, simple or cyclic voltammetry, use the synthesized Ppy/$I^-$ nanocomposite as a working electrode that is inserted into $Pb^{2+}$ solution at various concentrations. The sensor's sensitivity to $Pb^{2+}$ ions is validated by assessing its response to interfering ions. Furthermore, the sensor's effectiveness is assessed by testing it with real-world samples to observe how it behaves in practical situations. All of these measurements are conducted under typical environmental conditions and at room temperature.

These measurements provide us with a valuable indicator of the concentration of $Pb^{2+}$ ions, and this connection is established twice through the fundamental electrostatic interactions between the sensor and heavy metal ions to evaluate the reproducibility and accuracy. In simpler terms, as the concentration of heavy metals, such as lead ($Pb^{2+}$ ions), increases in solution, there is a proportional generation of additional electric charge. This generated charge is then detected by the evaluation of the electrical potential of the system.

The underlying principle behind this phenomenon is the strong attraction between the heavy metal ions and the sensor's surface. When heavy metal ions, like $Pb^{2+}$, are present in the solution, they interact with the sensor's surface due to their opposite charges, forming an electric double layer. As the heavy metal concentration increases, the electric double layer becomes more pronounced, leading to an increase in the potential difference detected by the sensor.

This approach is widely used in various analytical techniques, such as electrochemical sensors, for the precise quantification of heavy metal ions in environmental samples, industrial processes, and so on. By monitoring the changes in the evaluated potential, we can determine the concentration of $Pb^{2+}$ ions, making it an invaluable tool for environmental monitoring and quality control in diverse industries.

# 3 Results and discussion

Following the synthesis of both Ppy and PPy/$I^-$ nanocomposites, a comprehensive characterization is conducted to assess their chemical, morphological, and electrical properties. Subsequently, a PPy/$I^-$ thin film is employed for the detection of $Pb^{2+}$ ions utilizing two methods: a straightforward potentiometric approach and cyclic voltammetry. The sensor is subsequently employed for the detection of $Pb^{2+}$ ions in samples derived from natural sources.

## 3.1 Analyses

FTIR analysis provides valuable information about the characteristic functional groups present in Ppy and Ppy/$I^-$ nanomaterials. In Figure 1, the black and red curves represent the spectra of Ppy and Ppy/$I^-$ nanomaterials, respectively. Although they are similar, there are slight shifts in the peak positions, indicating the influence of iodide ions on the active sites of Ppy.

For the Ppy polymer, several main functional groups can be identified. The C═C bond vibrations are observed at 1,699 $cm^{-1}$ for the quinoid state and 1,545 $cm^{-1}$ for the benzene state. The N–H group is detected at 3,402 $cm^{-1}$. Additionally, the C–N bond vibration is observed at 1,312 $cm^{-1}$, and the C–H group is present at 1,177 $cm^{-1}$.

In the Ppy/$I^-$ nanomaterials, these functional groups are also present, but with small shifts in their positions due to the interaction with iodide ions. The specific positions of these functional groups in the FTIR spectra are given in Table 1, which provides a comprehensive overview of their positions and changes.

The XRD patterns of Ppy and Ppy/$I^-$ nanomaterials exhibit similar characteristics, indicating the structural nature of these materials.

Ppy shows an amorphous structure, as evidenced by a broad peak with a small semi-sharp peak observed at 26.6°. On the other hand, Ppy/$I^-$ nanomaterials exhibit a similar behavior with a small peak at 25.3°, indicating a semi-crystalline structure.

The crystal size ($D$) of the nanomaterials can be evaluated using equation (1) [19,20], which takes into account the peak angle and the full-width half-maximum of the peak (ß). Through this equation, the wavelength ($\lambda$) of the incidence XRD is 0.154 nm. Based on this calculation, the crystal size is determined to be 85 nm, using the peak at $2\theta$ of 25.3° for the Ppy/$I^-$ nanomaterials:

$$D = \frac{0.94\lambda}{ß\cos\theta}. \quad (1)$$

**Table 1:** FTIR analyzed data for Ppy and Ppy/$I^-$

| Position ($cm^{-1}$) | | Group |
|---|---|---|
| **Ppy/$I^-$** | **Ppy** | |
| 3,370 | 3,402 | N–H |
| 1,658 | 1,699 | Quinoid C═C |
| 1,535 | 1,545 | Benzene C═C [21] |
| 1,300 | 1,312 | C–N [22] |
| 1,167 | 1,177 | C–H |
| 899 | 910 | Para disubstituted ring |

The XPS analysis of Ppy/$I^-$ nanomaterials, as depicted in Figure 2, affirms the elemental composition of these materials. Notably, the nanomaterials demonstrate a high degree of purity for elements I, N, and C, with no discernible additional peaks that might suggest the presence of other elements, except for the O element, originating from the ethanol employed in the washing process.

Figure 2(b) specifically delineates the peaks associated with the element I, showcasing I $3d_{5/2}$ and I $3d_{3/2}$ peaks at 618 and 630 eV, respectively. These distinct peaks serve as clear indicators of the existence of I–N bonding within the formed nanomaterials, providing valuable insights into the structural composition.

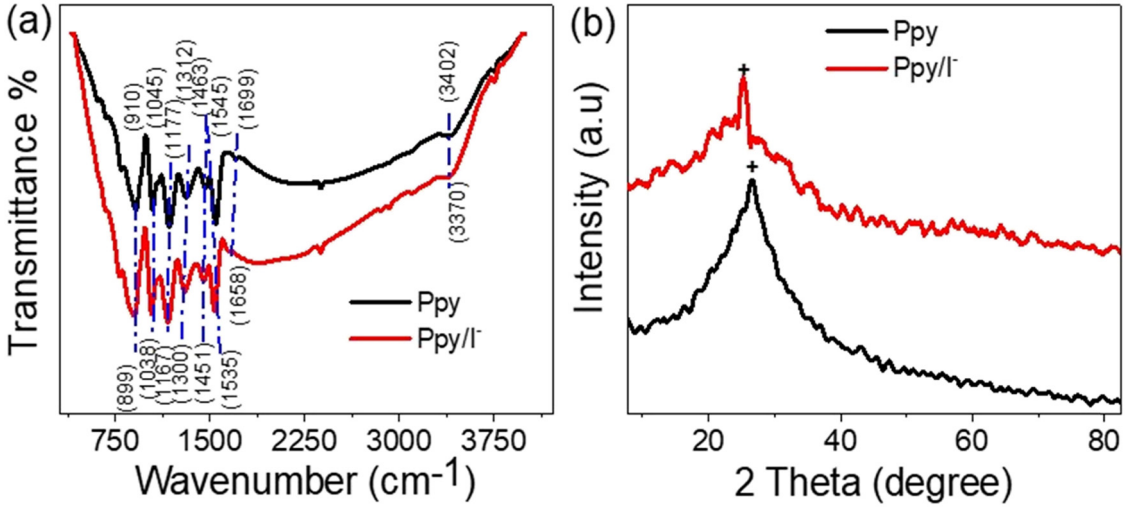


**Figure 1:** Characterization of the chemical structure using (a) FTIR and (b) XRD for Ppy and Ppy/$I^-$.

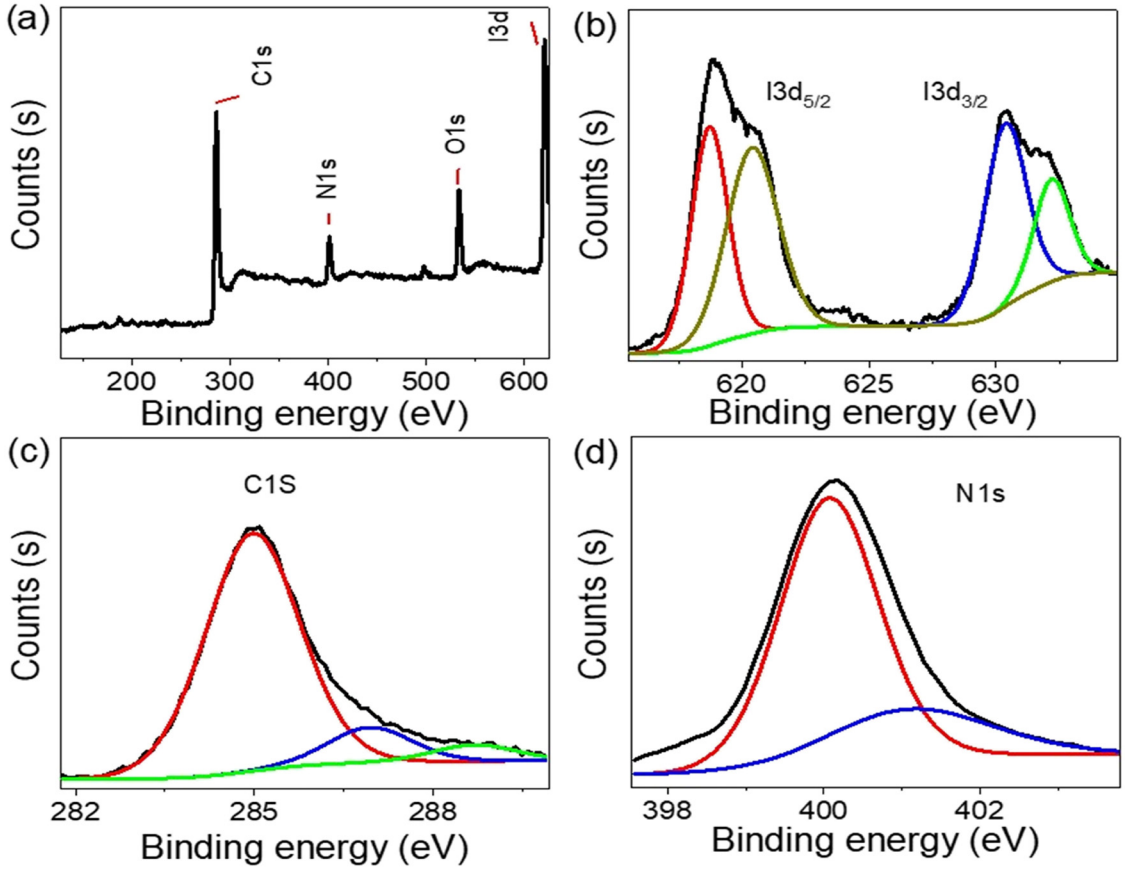


**Figure 2:** XPS analyses of the Ppy/$I^-$ nanomaterial: (a) survey, (b) I 3d, (c) C 1s, and (d) N 1s spectra.

As seen in Figure 2(c), the C1s spectra are situated at 285 eV. These peaks are attributed to the presence of C═C bonds within the benzene or quinone structures of the nanomaterials [23]. Additionally, any observed peaks may be attributed to the adsorption of $CO_2$ molecules from the surrounding environment, adding a layer of complexity to the analysis.

In Figure 2(d), the N 1 s spectra manifest at 400 eV and exhibit the active and positive sites within the Ppy nanomaterials. These spectra unequivocally indicate the presence of nitrogen (N) atoms within the structure, highlighting the incorporation of nitrogen in the nanomaterials. This presence of nitrogen is indicative of the potential role of nitrogen atoms in contributing to the overall functionality and reactivity of the Ppy nanomaterials.

Therefore, the XPS analysis of the Ppy/$I^-$ nanomaterials, as portrayed in Figure 2, provides a comprehensive understanding of the elemental composition and bonding characteristics. The presence of I–N bonding, C═C bonds and active nitrogen sites within the nanomaterials is elucidated through the examination of specific peaks, shedding light on the structural intricacies of the synthesized materials.

Figure 3 illustrates the distinctive morphological disparities between Ppy and Ppy/$I^-$ nanomaterials. In Figure 3(a), the Ppy nanomaterial exhibits a semi-spherical shape with a porous surface, and this porosity is evident within the particles themselves as well as between the granules. The average particle size measures approximately 250 nm. It is noteworthy that these semi-spherical particles are not hollow; they possess an internal structure. The unique morphological attributes, especially the porous surface, play a substantial role in enhancing the surface activity of the Ppy nanomaterial.

On the contrary, Ppy/$I^-$ nanomaterials assume a distinct mushroom-like configuration, featuring a noticeable cavity space within. This morphology is explicitly portrayed in the TEM image, where the inner diameter of the open-faced mushroom measures 250 nm, and the wall thickness is approximately 120 nm. SEM images in Figure 3(c) and (d) further emphasize this distinctive morphology, showcasing the formation of mushroom-shaped structures with conspicuous cavity surfaces and porous walls. This unique structure enables these materials to facilitate additional interactions through chemical reactions involving

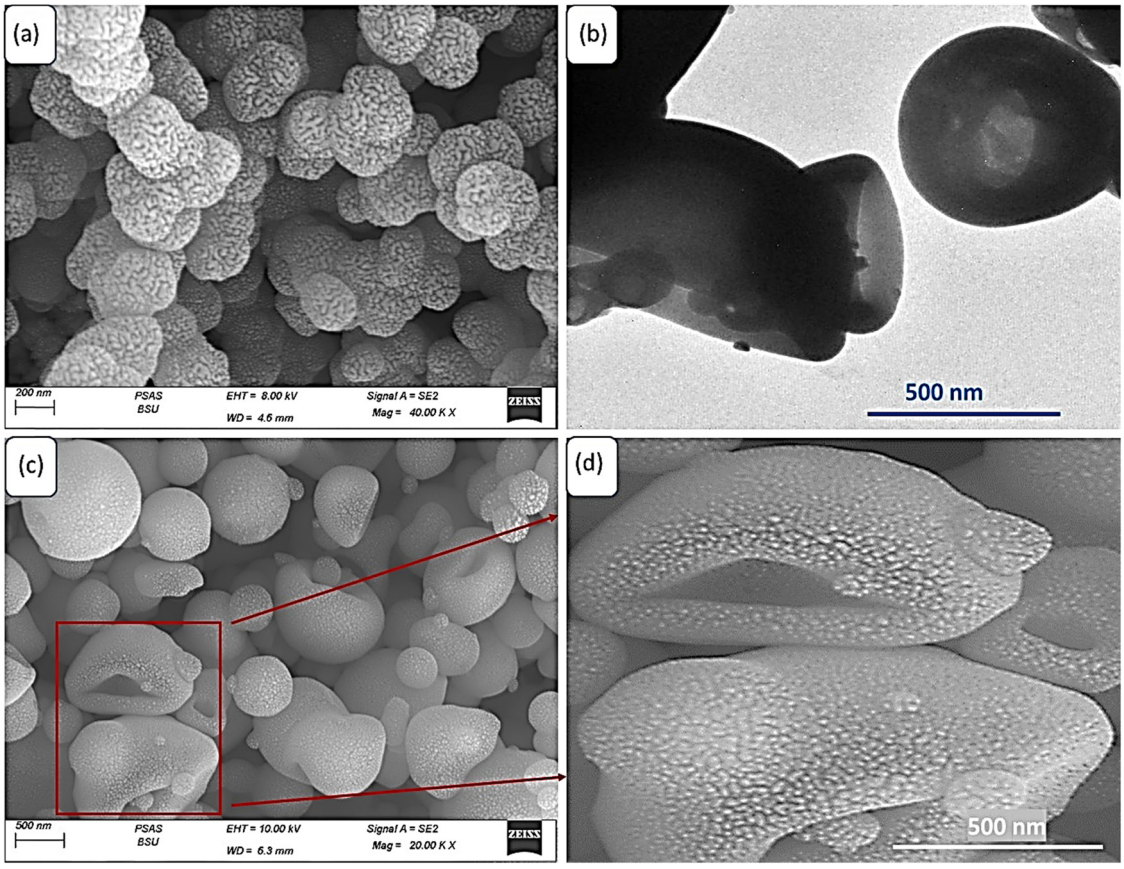


**Figure 3:** Morphological behavior of Ppy and Ppy/$I^-$: (a) SEM of Ppy, (b) TEM, and (c and d) SEM of Ppy/$I^-$ at different scale bars.

bond formation or electrostatic reactions based on charge interactions.

The unique structure of this polymer material imparts a variety of beneficial attributes, making it a versatile option for a wide range of applications. Its notable qualities make it particularly well-suited for various uses. A significant advantage lies in its considerable surface area, paving the way for improved performance, particularly in the detection of heavy metals. The existence of voids or empty spaces within this nanomaterial is a crucial aspect that adds to its heightened sensitivity.

In the specific domain of heavy metal detection, the polymer material's structure proves to be particularly advantageous. Its unique morphology, marked by substantial surface area and cavities, empowers it to excel in this application. The cavities within the nanomaterial are adept at efficiently engaging with heavy metal ions, thus elevating their ability to detect and quantify these metals with precision [24,25]. Furthermore, the economical nature of polymer materials and their straightforward preparation process, combined with their exceptional morphological characteristics, facilitate the expansion of active sites for metal detection [9,26–28]. This expansion occurs through the exchange of electrical charges, creating an attractive interaction between these metals and the active sites within the polymer. Collectively, these advantages make polymer materials a highly favorable choice for deploying them as sensors for heavy metals. Additionally, enhancing the performance of these sensors by introducing other ions, such as iodide, which intermingle with the polymer chains to provide an additional avenue for interaction with heavy metals, is regarded as a highly advantageous feature for these metal-detecting systems. Therefore, the distinctive morphology of this polymer material imparts a variety of promising characteristics, rendering it well-suited for a broad range of applications. Its substantial surface area and the existence of cavities contribute to an increased sensitivity, especially in the field of heavy metal detection. These nanomaterial cavities demonstrate efficiency in interacting with heavy metal ions, thereby strengthening their capabilities for precise detection and quantification of these metals monitoring.

## 3.2 Sensing properties

The Ppy/$I^-$ thin film sensor exhibits promising sensing behavior towards $Pb^{2+}$ ions, facilitated by the interaction between the $Pb^{2+}$ ions and the Ppy/$I^-$ nanomaterials. The excellent morphological properties of Ppy/$I^-$ contribute to significant enhancements in sensing performance, as observed in both simple and cyclic potentiometric studies.

In the simple potentiometric study, the sensitivity of the Ppy/$I^-$ sensor to $Pb^{2+}$ ions is measured using a two-electrode cell configuration. The Ppy/$I^-$ thin film serves as the main electrode, while a calomel electrode is used as the reference. The potential difference between these two electrodes reflects the sensing potential of the sensor towards $Pb^{2+}$ ions. The Nernstian slope, which has a theoretical value of 29.56 mV/decade [17,29], is used to calibrate the potential measurements. Measurements are conducted in a concentration range spanning from $10^{-8}$ to $10^{-1}$ M, maintaining a pH of 5.5. These experiments provide valuable insights into the sensing capabilities of the Ppy/$I^-$ sensor for $Pb^{2+}$ ions across a wide concentration range.

The calibration curve of $Pb^{2+}$ ions by Ppy/$I^-$ sensor, obtained through the simple potentiometric method, is depicted in Figure 4(a). The slope of the calibration curve is measured to be 31.7 mV/decade, which closely aligns with an optimum value of 29.56 mV/decade. This demonstrates the sensor's capability for efficient detection of $Pb^{2+}$ ions. The linear detection range of the sensor spans from $10^{-5}$ to $10^{-1}$ M, exhibiting high linearity within this concentration range. The detection limit of the sensor is determined to be $9 \times 10^{-6}$ M (<2 ppm), indicating its sensitivity to low concentrations of $Pb^{2+}$ ions. These findings highlight the excellent performance of the Ppy/$I^-$ sensor in detecting $Pb^{2+}$ ions, as demonstrated by the close alignment of the slope with the optimal value and the wide linear detection range [30,31]. Additionally, the low detection limit further

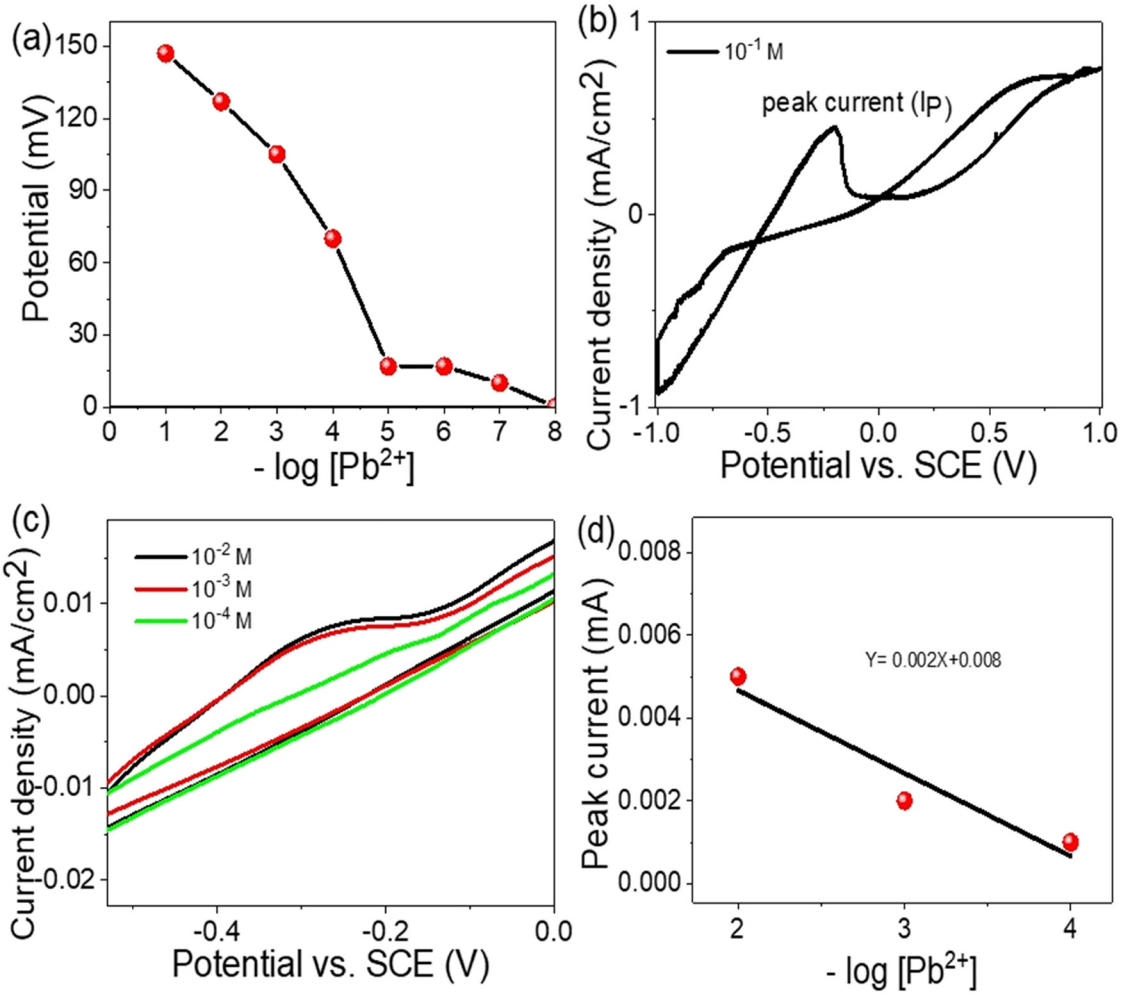


**Figure 4:** Ppy/$I^-$ sensor for $Pb^{2+}$ ions through (a) simple potentiometric and (b and c) cyclic voltammetry technique in a concentration range from $10^{-4}$ to $10^{-1}$ M, versus saturated calomel electrode (SCE), and (d) the sensitivity behavior through the relation of −log [$Pb^{2+}$] with the current density.

confirms the sensor's high sensitivity for accurate detection of $Pb^{2+}$ ions.

The cyclic voltammetry behavior of the Ppy/$I^-$ sensor for $Pb^{2+}$ ions was evaluated using a three-electrode cell configuration. The Ppy/$I^-$ sensor served as the main electrode, while the calomel and graphite electrodes functioned as the other two electrodes within the cell. Measurements were conducted over a concentration range spanning from $10^{-4}$ to $10^{-1}$ M at pH 5.5. In Figure 4(b), the cyclic voltammetry curve clearly illustrates a distinct peak corresponding to the detection of $Pb^{2+}$ ions at a potential of −0.2 V, indicating a strong sensing capability of the Ppy/$I^-$ sensor for $Pb^{2+}$ ions. Figure 4(c) further demonstrates the detection of $Pb^{2+}$ ions in a concentration range from $10^{-4}$ to $10^{-2}$ M, where the current density (*I*) increases with increasing concentrations from $10^{-4}$ to $10^{-2}$ M. The concentration-dependent response of the Ppy/$I^-$ sensor to $Pb^{2+}$ ions at low concentrations can be attributed to two main factors. First, the strong interaction between $Pb^{2+}$ ions and the Ppy/$I^-$ sensor occurs due to electrostatic phenomena. The electronegative atoms in the polymer and the positive charge of $Pb^{2+}$ ions lead to a favorable interaction, enhancing the sensitivity of the sensor toward $Pb^{2+}$ ions [32–34].

The distinctive morphology of the Ppy/$I^-$ sensor plays a crucial role in its responsiveness to $Pb^{2+}$ ions. This sensor boasts a highly porous structure with prominent cavities on its surface, which facilitate the diffusion and dispersion of $Pb^{2+}$ ions within these features. This particular morphology offers additional surface area, allowing for efficient capture and detection of $Pb^{2+}$ ions, resulting in the heightened sensitivity observed at low concentrations [33,41].

Several factors contribute to the concentration-dependent response of the Ppy/$I^-$ sensor to $Pb^{2+}$ ions, especially at low concentrations. One key factor is the electrostatic interaction between the sensor and the ions, which helps attract and bind $Pb^{2+}$ ions to the sensor's surface. This interaction is further aided by the favorable morphology of the sensor, with its porous structure creating an environment conducive to ion binding [25,35].

The cavities within the Ppy/$I^-$ sensor significantly increase the available surface area and the number of active sites for ion binding. This morphological feature essentially acts as a trap for $Pb^{2+}$ ions, enhancing the sensor's ability to sense their charge. The unique structure of the sensor promotes the efficient interaction between $Pb^{2+}$ ions and the sensor surface, leading to a more pronounced response to changes in the $Pb^{2+}$ ion concentration.

Therefore, the remarkable morphology of the Ppy/$I^-$ sensor, characterized by its porous structure and cavity-rich surface, plays a pivotal role in its sensitivity to $Pb^{2+}$ ions. This distinctive morphology not only increases the surface area but also acts as an effective trap for $Pb^{2+}$ ions, contributing to the sensor's concentration-dependent response and making it particularly effective at low $Pb^{2+}$ ion concentrations.

The sensitivity of the Ppy/$I^-$ sensor to $Pb^{2+}$ ions is quantified in Figure 4(d), with a slope of 2 μA/M. Although these values may appear to be small, they indicate the wide sensitivity range of the sensor toward $Pb^{2+}$ ions, further affirming its suitability for efficient detection of $Pb^{2+}$ ions, matching our previous work [34,36].

The effect of interfering ions on the responsiveness of the Ppy/$I^-$ sensor for $Pb^{2+}$ ions was investigated and is presented in Figure 5(a). The measurements were conducted using the three-electrode cell mentioned earlier, with the interfering ions (potassium ($K^+$), magnesium

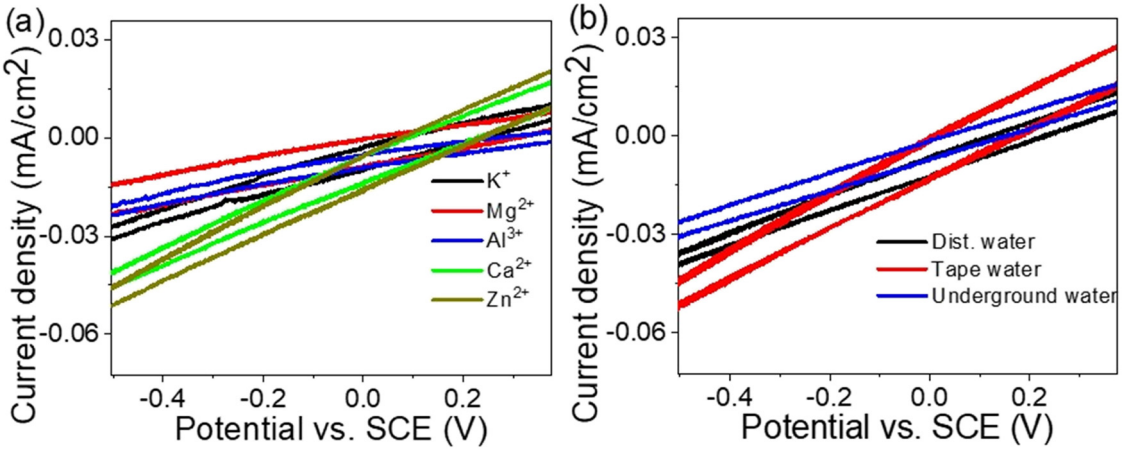


**Figure 5:** Ppy/$I^-$ sensor used to test the (a) interfering ions and (b) natural samples through the potential versus SCE with the current density values produced.

($Mg^{2+}$), aluminum ($Al^{3+}$), calcium ($Ca^{2+}$), or zinc ($Zn^{2+}$)) present at a concentration of 0.01 M and pH 5.5. It was observed that the Ppy/$I^-$ sensor exhibited a negative response to these interfering ions, with no characteristic peaks observed for their detection.

Figure 5(b) further demonstrates the responsiveness of the Ppy/$I^-$ sensor to various elements present in tap or underground water (specifically from Beni-Suef City, Egypt), using distilled water as a reference. The Ppy/$I^-$ sensor showed a negative response to these elements, indicating its selectivity toward $Pb^{2+}$ ions.

The results of these investigations serve to emphasize the exceptional sensitivity and selectivity of the Ppy/I-sensor in its response to $Pb^{2+}$ ions. Even in the presence of interfering ions and various elements commonly encountered in natural water samples, whether sourced from tap water or underground reservoirs, the sensor consistently retained its proficiency in precisely identifying $Pb^{2+}$ ions. Furthermore, it consistently displayed a counteractive response when confronted with the interfering ions that were subjected to testing. Therefore, these findings reaffirm the outstanding sensitivity and selectivity of the Ppy/$I^-$ sensor when it comes to the detection of $Pb^{2+}$ ions. These attributes solidify its position as a reliable choice for practical applications that necessitate accurate detection and quantification of $Pb^{2+}$ ions while effectively mitigating the influence of interference from other ions and elements.

Overall, these results confirm the high sensitivity and selectivity of the Ppy/$I^-$ sensor for $Pb^{2+}$ ions, making it a reliable choice for practical applications requiring accurate detection and measurements of $Pb^{2+}$ ions while minimizing interference from other ions or elements.

## 4 Conclusions

The use of Ppy/$I^-$ nanomaterials for potentiometric sensing of $Pb^{2+}$ ions in water is achieved by employing an iodine oxidant on the pyrrole monomer. The resulting Ppy/$I^-$ nanomaterials exhibit a unique and visually appealing morphology, resembling hollow mushrooms with a face cavity measuring 250 nm and a wall thickness of 120 nm, exhibiting additional porous characteristics.

When applied for $Pb^{2+}$ determination, the Ppy/$I^-$ sensor demonstrates a promising Nernstian slope of 31.7 mV/decade, indicating a linear response over the concentration range of $10^{-5}$–$10^{-1}$ M, with a detection limit of $9 \times 10^{-6}$ M. This performance is supported by cyclic voltammetry analysis, where a distinct potential peak at −0.2 V is observed for $Pb^{2+}$ sensing using the Ppy/$I^-$ sensor. The sensor exhibits a sensitivity of 2 μA/M in this regard.

Furthermore, the Ppy/$I^-$ sensor displays a negative response to interfering ions, showcasing its selectivity for $Pb^{2+}$ detection. Moreover, even in the presence of normal interfering ions typically found in natural water samples, such as tap or underground water, which are devoid of lead ions, the sensor maintains a negative response. Overall, this Ppy/$I^-$ sensor offers advantages such as the ability to detect trace amounts of $Pb^{2+}$ ions, flexibility in its application, and a cost-effective preparation method. These qualities make it a highly promising tool for accurate and adaptable detection of $Pb^{2+}$ ions at very low concentrations.

**Acknowledgments:** This work was financially supported by Princess Nourah bint Abdulrahman University Researchers Supporting Project number (PNURSP2024R186), Princess Nourah bint Abdulrahman University, Riyadh, Saudi Arabia.

**Funding information:** This work was financially supported by Princess Nourah bint Abdulrahman University Researchers Supporting Project number (PNURSP2024R186), Princess Nourah bint Abdulrahman University, Riyadh, Saudi Arabia.

**Author contributions:** M.R.: experimental, analyses, and writing; M.A.A: writing, supervision, revision, and ordering the work.

**Conflict of interest:** The authors have no conflict of interest.

**Ethical Approval:** This study does not include any human or animal studies.

**Data availability statement:** All data generated or analyzed during this study are included in this article.

## References

[1] El-Fatah GA, Magar HS, Hassan RYA, Mahmoud R, Farghali AA, Hassouna MEM. A novel gallium oxide nanoparticles-based sensor for the simultaneous electrochemical detection of Pb2+, Cd2+ and Hg2+ ions in real water samples. Sci Rep. 2022;12:1–14. doi: 10.1038/s41598-022-24558-y.

[2] Yan J, He Y, Chen Y, Zhang Y, Yan H. CH3NH3Br solution as a novel platform for the selective fluorescence detection of $Pb^{2+}$ ions. Sci Rep. 2019;9:1–7. doi: 10.1038/s41598-019-52431-y.

[3] Wang Y, Xu L, Shen H, Wang J, Liu W, Zhu X, et al. Metabolomic analysis with GC-MS to reveal potential metabolites and biological pathways involved in Pb & Cd stress response of radish roots. Sci Rep. 2015;5:1–13. doi: 10.1038/srep18296.

[4] Liu L, Ye K, Lin C, Jia Z, Xue T, Nie A, et al. Grain-boundary-rich polycrystalline monolayer WS2 film for attomolar-level Hg2+ sensors. Nat Commun. 2021;12:1–8. doi: 10.1038/s41467-021-24254-x.

[5] Wang H, Huang X, Wen G, Jiang Z. A dual-model SERS and RRS analytical platform for Pb(II) based on Ag-doped carbon dot catalytic amplification and aptamer regulation. Sci Rep. 2019;9:1–10. doi: 10.1038/s41598-019-46426-y.
[6] Alboghbeish M, Larki A, Saghanezhad SJ. Effective removal of Pb(II) ions using piperazine-modified magnetic graphene oxide nanocomposite; optimization by response surface methodology. Sci Rep. 2022;12:1–17. doi: 10.1038/s41598-022-13959-8.
[7] Wang B, Thukral A, Xie Z, Liu L, Zhang X, Huang W, et al. Flexible and stretchable metal oxide nanofiber networks for multimodal and monolithically integrated wearable electronics. Nat Commun. 2020;11:1–11. doi: 10.1038/s41467-020-16268-8.
[8] Alruqi M, Rabia M, Elsayed AM, Hanafi HA, Shaban M, Hamid MMA. Development of polypyrrole/Ni(OH)2-NiO core-shell nanocomposite as an optoelectronic device. J Appl Polym Sci. 2023;140:e53833. doi: 10.1002/APP.53833.
[9] Wan Y, Jiang H, Ren Y, Liu Y, Zhang L, Lei Q, et al. Photothermal self-healable polypyrrole-polyurethane sponge with dynamic covalent oximino bonds for flexible strain sensors. Eur Polym J. 2023;193:112097. doi: 10.1016/J.EURPOLYMJ.2023.112097.
[10] Mei X, Wang X, Huang W, Zhu J, Liu K, Wang X, et al. A novel polycaprolactone/polypyrrole/β-cyclodextrin electrochemical flexible sensor for dinotefuran pesticide detection. Food Chem. 2024;434:137194. doi: 10.1016/J.FOODCHEM.2023.137194.
[11] Ratautaite V, Boguzaite R, Brazys E, Ramanaviciene A, Ciplys E, Juozapaitis M, et al. Molecularly imprinted polypyrrole based sensor for the detection of SARS-CoV-2 spike glycoprotein. Electrochim Acta. 2022;403:139581. doi: 10.1016/J.ELECTACTA.2021.139581.
[12] Jain A, Nabeel AN, Bhagwat S, Kumar R, Sharma S, Kozak D, et al. Fabrication of polypyrrole gas sensor for detection of NH3 using an oxidizing agent and pyrrole combinations: Studies and characterizations. Heliyon. 2023;9:e17611. doi: 10.1016/J.HELIYON.2023.E17611.
[13] Triviño JJ, Núñez C, Martín IMS, Zúñiga M, Arancibia V. Voltammetric method for the determination of Pb2+ and Cd2+ in water samples using a nafion−guanine-coated mercury film electrode. Int J Electrochem Sci. 2022;17:220762. doi: 10.20964/2022.07.71.
[14] Ghaedi M, Montazerozohori M, Andikaey Z, Shokrollahi A, Khodadoust S, Behfar M, et al. Fabrication of Pb2+ ion selective electrode based on 1-((3-((2-hydroxynaphthalen-1-Yl)methyleneamino)-2,2-dimethylpropylimino) Methyl) naphthalen-2-Ol as new neutral ionophore. Int J Electrochem Sci. 2011;6:4127–40. doi: 10.1016/S1452-3981(23)18315-5.
[15] Ikena H, Kirsanov D, Legin A, Schöning MJ. Novel thin-film polymeric materials for the detection of heavy metals. Procedia Eng. 2012;47:322–5. doi: 10.1016/J.PROENG.2012.09.148.
[16] Khalil MM, Issa YM, Zayed SIM, Ali FQ. New potentiometric membrane sensors for determination of alverine citrate in pharmaceutical compounds and biological fluids. Int J Adv Res. 2014;2:1096–109.
[17] Khalil MM, Farghali AA, El Rouby WMA, Abd-Elgawad IH. Preparation and characterization of novel MWCNTs/Fe-Co doped TNTs nanocomposite for potentiometric determination of sulpiride in real water samples. Sci Rep. 2020;10:8607. doi: 10.1038/S41598-020-65592-Y.
[18] Rabia M, Elsayed AM, Salem AM, Abdallah Alnuwaiser M. Highly uniform multi-layers reduced graphene oxide/poly-2-aminobenzene-1-thiol nanocomposite as a promising two electrode symmetric supercapacitor under the effect of absence and presence of porous-sphere polypyrrole nanomaterial. Micromachines. 2023;14:1424. doi: 10.3390/MI14071424.
[19] Rajeevgandhi C, Sathiyamurthy K, Guganathan L, Savithiri S, Bharanidharan S, Mohan K. Experimental and theoretical investigations on the spinel structure of Co2O3 nanoparticles synthesized via simple co-precipitation method. J Mater Sci.: Mater Electron. 2020;31:16769–79. doi: 10.1007/S10854-020-04232-7/TABLES/5.
[20] Noori SM. Synthesis and characterization of Ni-Si 3 N 4 nanocomposite coatings fabricated by pulse electrodeposition. Bull Mater Sci. 2034;42:44. doi: 10.1007/s12034-019-1733-4.
[21] Azzam EMS, Abd El-Salam HM, Aboad RS. Kinetic preparation and antibacterial activity of nanocrystalline poly(2-Aminothiophenol). Polym Bull. 2019;76:1929–47. doi: 10.1007/S00289-018-2405-Z/FIGURES/14.
[22] Boomi P, Anandha Raj J, Palaniappan SP, Poorani G, Selvam S, Gurumallesh Prabu H, et al. Improved conductivity and antibacterial activity of poly(2-aminothiophenol)-silver nanocomposite against human pathogens. J Photochem Photobiol B: Biol. 2018;178:323–9. doi: 10.1016/J.JPHOTOBIOL.2017.11.029.
[23] Rabia M, Elsayed AM, Alnuwaiser MA. Decoration of poly-3-methyl aniline with As(III) oxide and hydroxide as an effective photoelectrode for electroanalytical photon sensing with photodiode-like behavior. Micromachines. 2023;14:1573. doi: 10.3390/MI14081573.
[24] Motsoeneng RG, Kortidis I, Rikhotso R, Swart HC, Ray SS, Motaung DE. Temperature-dependent response to C3H7OH and C2H5OH vapors induced by deposition of au nanoparticles on SnO2/NiO hollow sphere-based conductometric sensors. Sens Actuators B: Chem. 2020;316:128041. doi: 10.1016/J.SNB.2020.128041.
[25] Muhammad Hafiz S, Ritikos R, Whitcher TJ, Md, Razib N, Bien DCS, et al. A practical carbon dioxide gas sensor using room-temperature hydrogen plasma reduced graphene oxide. Sens Actuators B: Chem. 2014;193:692–700. doi: 10.1016/j.snb.2013.12.017.
[26] Srinivasan P, Madhu DK, Pedugu Sivaraman S, Nagarajan S, Rao CVSB, Chinaraga PK, et al. Chromoionophoric probe imbued porous polymer monolith as a three-in-one solid-state naked-eye sensor for the selective sensing and recovery of ultra-trace lead, mercury, and cadmium ions from industrial/environmental samples. Chem Eng J. 2023;471:144627. doi: 10.1016/J.CEJ.2023.144627.
[27] Liu C, Wu M, Gao L, Liu H, Yu J. Nanoporous polymer films based on breath figure method for stretchable chemiresistive NO2 gas sensors. Sens Actuators B: Chem. 2022;371:132540. doi: 10.1016/J.SNB.2022.132540.
[28] Cui M, Xie Z, Wang M, Zhang X. Methyl orange-crosslinked polypyrrole hydrogel enabled N, O, S Co-doped porous carbon for highly sensitive determination of three redox-active biomolecules. J Electroanal Chem. 2022;913:116282. doi: 10.1016/J.JELECHEM.2022.116282.
[29] Khalil MM, El Rouby WMA, Korany MA. Potentiometric sensor based on novel flowered-like Mg-Al layered double hydroxides/multiwalled carbon nanotubes nanocomposite for bambuterol hydrochloride determination. Mater Sci Eng C. 2019;100:186–95. doi: 10.1016/j.msec.2019.02.103.

[30] Saleh M, Khalil M, Abdellateif MS, Ebeid E, Madney Y, Kandeel EZ. Role of matrix metalloproteinase MMP-2, MMP-9 and tissue inhibitor of metalloproteinase (TIMP-1) in the clinical progression of pediatric acute lymphoblastic leukemia. Hematology. 2021;26:758–68. doi: 10.1080/16078454.2021.1978763.

[31] Ebrahim S, Shokry A, Khalil MMA, Ibrahim H, Soliman M. Polyaniline/Ag nanoparticles/graphene oxide nanocomposite fluorescent sensor for recognition of chromium (VI) ions. Sci Rep. 2020;10:1–11. doi: 10.1038/s41598-020-70678-8.

[32] Zaki SE, Basyooni MA, Shaban M, Rabia M, Eker YR, Attia GF, et al. Role of oxygen vacancies in vanadium oxide and oxygen functional groups in graphene oxide for room temperature CO2 gas sensors. Sens Actuators A: Phys. 2019;294:17–24. doi: 10.1016/J.SNA.2019.04.037.

[33] Sayyah SM, Shaban M, Rabia M. A high-sensitivity potentiometric mercuric ion sensor based on m-toluidine films. IEEE Sens J. 2016;16:1541–8. doi: 10.1109/JSEN.2015.2505313.

[34] Sayyah E-SM, Shaban M, Rabia M. A sensor of M-cresol nanopolymer/Pt-electrode film for detection of lead ions by potentiometric methods. Adv Polym Technol. 2016;37(5):1296–304. doi: 10.1002/adv.21788.

[35] Sabah FA, Ahmed NM, Hassan Z, Almessiere MA. Influence of CuS membrane annealing time on the sensitivity of EGFET PH sensor. Mater Sci Semicond Process. 2017;71:217–25. doi: 10.1016/j.mssp.2017.07.001.

[36] Sayyah SM, Shaban M, Rabia M. A sensor of M-Toluidine/m-cresol polymer film for detection of lead ions by potentiometric methods. Sens Lett. 2016;14:522–9. doi: 10.1166/sl.2016.3656.